Continuous and Discontinuous Dynamic Unbinding Transitions in Drawn Film Flow

M. Galvagno,[1,*] D. Tseluiko,[1] H. Lopez,[2] and U. Thiele[1,3,†]
[1]Department of Mathematical Sciences, Loughborough University, Loughborough, Leicestershire LE11 3TU, United Kingdom
[2]School of Physics and Complex and Adaptive Systems Laboratory, University College Dublin, Belfield, Dublin 4, Ireland
[3]Institut für Theoretische Physik, Westfälische Wilhelms-Universität Münster, Wilhelm Klemm Strasse 9, D-48149 Münster, Germany
(Received 28 November 2013; published 4 April 2014)

When a plate is withdrawn from a liquid bath a coating layer is deposited whose thickness and homogeneity depend on the velocity and the wetting properties of the plate. Using a long-wave mesoscopic hydrodynamic description that incorporates wettability via a Derjaguin (disjoining) pressure we identify four qualitatively different dynamic transitions between microscopic and macroscopic coatings that are out-of-equilibrium equivalents of known equilibrium unbinding transitions. Namely, these are continuous and discontinuous dynamic wetting and emptying transitions. Several of their features have no equivalent at equilibrium.

DOI: 10.1103/PhysRevLett.112.137803 PACS numbers: 68.15.+e, 47.20.Ky, 47.55.D-, 68.08.-p

The equilibrium and nonequilibrium behavior of mesoscopic and macroscopic drops, menisci, and films of liquid in contact with static or moving solid substrates is not only of fundamental interest but also crucial for a large number of modern technologies. On the one hand, the equilibrium behavior of films, drops, and menisci is studied by means of statistical physics. A rich substrate-induced phase transition behavior is described even for simple liquids, e.g., related to wetting and emptying transitions—both represent unbinding transitions well studied at equilibrium. In a wetting transition, the thickness of an adsorption layer of liquid diverges continuously or discontinuously at a critical temperature or strength of substrate-liquid interaction; i.e., the liquid-gas interface of the film unbinds from the liquid-solid interface [1]. In an emptying transition, a macroscopic meniscus in a tilted slit capillary develops a tongue (or foot) along the lower wall. The foot length diverges logarithmically at a critical slit width; i.e., the tip of the foot unbinds from the meniscus and the capillary is emptied [2].

On the other hand, it is a classical hydrodynamic problem to study how droplets slide down an incline [3–6], how moving contact lines (where solid, gas and liquid meet) develop sawtooth shapes at high speeds [6–8], or how the free surface of a bath is deformed when a plate is drawn out, as sketched in Fig. 1(a). Early on it was reported that for sufficiently large plate velocities U a homogeneous macroscopic liquid layer is deposited on the plate [Fig. 1(d)]. The resulting coating layer is called a Landau-Levich film. Far away from the bath its thickness h_∞ depends on the capillary number $\mathrm{Ca} = \eta U/\gamma$ through the power law $h_\infty \propto \mathrm{Ca}^{2/3}$ [9] where η and γ are the viscosity and surface tension of the liquid, respectively. This coating technique is widely used and became a paradigm for theoretical (e.g., Refs. [6,9–12]) and experimental (e.g., Refs. [13–17]) studies.

In contrast, at very low plate velocities U no macroscopic film is drawn out but a deformed steady meniscus coexists with the dry plate far away from the bath [8,16,18–20] [Fig. 1(b)]. This meniscus only exists for capillary numbers smaller than a critical one, Ca_c [18]. Close to Ca_c the meniscus develops a foot of a length L_f [Fig. 1(c)] that diverges at Ca_c either continuously [21] or discontinuously [19]. As the steady free surface meniscus coexists with the dry moving plate, there exists a receding three-phase contact line whose best description is still debated (see, e.g., Refs. [1,22,23]).

Previous works [18,19,21] employ a slip model that allows the film height to go to zero at the contact line and avoids the contact line singularity through the slip [1]. Although a slip model allows for individual quantitative studies of meniscus solutions and Landau-Levich films, it is not able to describe transitions between them, as in a slip model they are topologically different. Namely, for

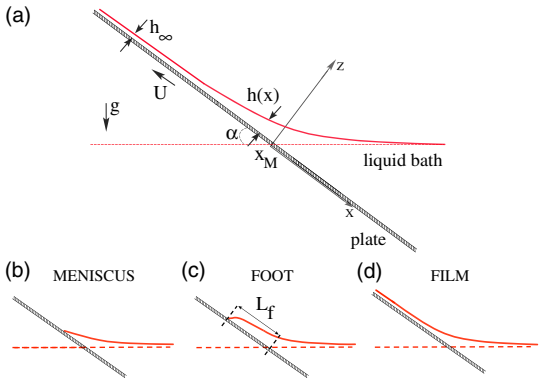

FIG. 1 (color online). Sketches of (a) the considered two-dimensional geometry and (b)–(d) of the qualitatively different steady shapes $h(x)$ of the free liquid surface as found in experiments: (b) simple meniscus, (c) foot or extended meniscus, and (d) Landau-Levich film. In (a) a flat plate inclined at an angle α to the horizontal is drawn out of a bath of a nonvolatile partially wetting liquid at a speed U.

meniscus and foot solutions the film height goes exactly to zero at the contact line, whereas for film solutions the coating thickness approaches a constant value at infinity, and there is no way to continuously transform one type of solutions into another [cf. Figs. 1(b) and 1(c) vs Fig. 1(d)]. Note that this concerns the actual transition dynamics as well as the description of transitions in dependence of control parameters such as the plate speed.

In contrast, here we employ a long-wave mesoscopic hydrodynamic model that describes wettability via a Derjaguin (disjoining) pressure, i.e., a precursor film model. An investigation of the nonequilibrium transitions between meniscus solutions and Landau-Levich films then allows for an identification of four qualitatively different dynamic unbinding transitions, namely, continuous and discontinuous dynamic wetting and emptying transitions. Note that far from the transition regions, the predictions of precursor and slip models agree very well and can be quantitatively mapped [24].

In particular, we use the following nondimensionalized evolution equation for the film thickness profile $h(x,t)$ [22,25,26]:

$$\partial_t h = -\partial_x\{h^3\partial_x[\partial_x^2 h + \Pi(h)] - h^3 G(\partial_x h - \alpha) - Uh\}, \quad (1)$$

that may be derived as long-wave approximation of the Navier-Stokes and continuity equations with no-slip conditions at the liquid-solid interface and kinematic and stress balance conditions at the liquid-gas interface [27]. Here U, G, and α are the dimensionless parameters that represent plate velocity (Capillary number), gravity (Bond number), and the scaled $O(1)$ inclination angle of the plate, respectively (see note [28]). The wettability of the partially wetting liquid is described via the Derjaguin pressure [29]

$$\Pi = -\frac{1}{h^3}\left(1 - \frac{1}{h^3}\right), \quad (2)$$

derived in Ref. [30] from a modified Lennard-Jones potential with hard-core repulsion (see note [28]). The disjoining pressure is related to a wetting or adhesion energy $f(h)$ via $\Pi = -df/dh$. The employed scales are $\ell = \sqrt{3/5}h_{\rm eq}/\theta_{\rm eq}$, $h_{\rm eq}$ and $\tau = (3\eta h_{\rm eq})/(25\gamma\theta_{\rm eq}^4)$ for the x coordinate, film height, and time, respectively, where $h_{\rm eq}$ and $\theta_{\rm eq}$ are the equilibrium precursor height and contact angle, respectively (cf. note [28]).

It should be noted that the hydrodynamic long-wave model, Eq. (1) with Eq. (2), directly corresponds to a gradient dynamics of an underlying interface Hamiltonian (or free energy) $F[h] = \int[\xi\gamma + f(h)]dx$ as often used to study the above introduced equilibrium unbinding transitions (cf. note [31]). This equivalence allows for a natural understanding of the various occurring transitions as nonequilibrium (or dynamic) unbinding transitions.

To obtain steady film and meniscus profiles, we solve the steady version of Eq. (1) requiring that far from the bath the film thickness approaches a constant value h_∞ and that the approach towards the bath is described by an asymptotic series rigorously derived via a center manifold reduction [32]. Steady profiles and bifurcation diagrams are numerically obtained employing pseudo-arclength continuation [33]. The main solution measure is the dynamic excess volume $\Delta V = V - V_0$ with $V = \int(h(x) - h_\infty)dx$, where V_0 is V at $U = 0$. Note that for solutions with a long protruding foot-like structure, ΔV is approximately proportional to the length of the foot [34].

An analysis of the changes that steady menisci undergo with increasing plate speed U shows that four qualitatively different cases exist depending on the plate inclination angle α. Each case is related to a distinguished nonequilibrium unbinding transition as illustrated in Fig. 2.

(a) At small α, the volume ΔV monotonically increases: first slowly, then faster until it diverges at $U_\infty \approx 0.04$ [Fig. 2(a)]. The corresponding simple meniscus profiles first deform only slightly due to viscous bending before a distinguished footlike protrusion of a height $h_f \approx 10$ develops whose length L_f diverges $\propto \ln[(U_\infty - U)/U_\infty]^{-1}$. This corresponds to a *continuous dynamic emptying transition*, a nonequilibrium analogue of the equilibrium transition discussed above (cf. Ref. [2]). In other words, at U_∞ the tip of the foot unbinds from the meniscus and the bath is emptied. For $U > U_\infty$, the foot advances with a constant velocity

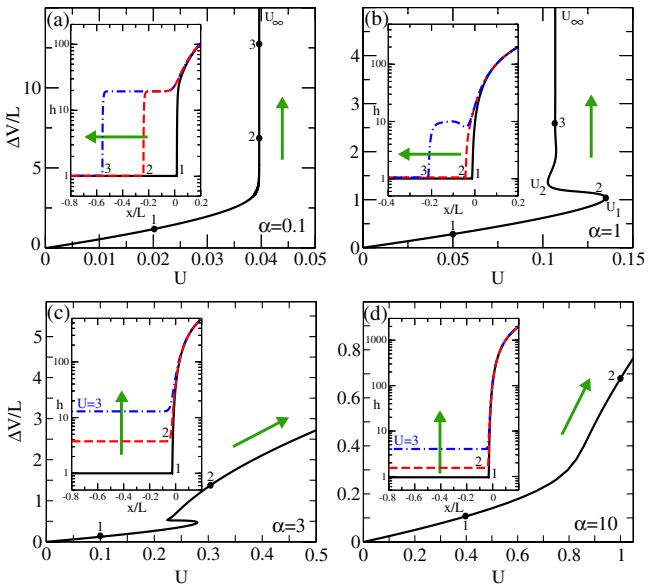

FIG. 2 (color online). Bifurcation curves showing qualitatively different behavior with increasing plate inclination angles (a) $\alpha = 0.1$, (b) $\alpha = 1$, (c) $\alpha = 3$, and (d) $\alpha = 10$. The main panels show $\Delta V/L$ in dependence on the plate velocity U, where $L = 1000$ is the domain size. The insets give log-normal representations of steady film profiles as indicated by corresponding labels.

$V_F \approx (U - U_\infty)$ as shown in Fig. 3, in a finite system, ultimately resulting in a Landau-Levich film state.

(b) Above a first critical $\alpha = \alpha_1 \approx 0.103$, the transition changes its character and becomes a *discontinuous dynamic emptying transition* that has no analogue at equilibrium. As shown in Fig. 2(b), ΔV increases first monotonically with U until a saddle-node bifurcation is reached at U_1 where the curve folds back. Following the curve further, one finds that it folds again at U_2. This back and forth folding infinitely continues at loci that exponentially approach U_∞ from both sides and that separate linearly stable and unstable parts of the solution branch. This exponential (or collapsed) snaking [36] results in a foot length with $[(U_\infty - U)/U_\infty]^{-1} \propto \exp(\mathrm{Re}[\nu]L_f) \times \sin(\mathrm{Im}[\nu]L_f)$ where ν is a linear eigenvalue whose real and imaginary part determine the exponential approach and the period of the snaking, respectively [32]. Note that for $U > U_\infty$ one can always find a critical foot length beyond which the foot advances with a constant velocity $V_F \approx (U - U_\infty)$, ultimately resulting in a film state. In contrast, for $U < U_\infty$ there is always a critical length above which a foot recedes. Advancing and receding fronts are illustrated in Fig. 3(a) for $\alpha = 0.1$, 0.2 and 0.5. Panels (b) and (c) show for $\alpha = 0.5$ the time evolution [35] of a receding and an advancing foot, respectively. In both previously described regions, (a) and (b), one finds that $h_f \propto {U_\infty}^{1/2}$. The limiting velocity U_∞^α coincides with the velocity of a large flat drop (pancakelike drop) sliding down a resting plate of inclination α [4]. This allows one to calculate U_∞ by continuation (see Fig. 5 below). Note that the found relation for the front velocity $V_F \approx U - U_\infty^\alpha$ [Fig. 3(a)] is a direct consequence of the Galilean invariance of the motion of a drop down an incline.

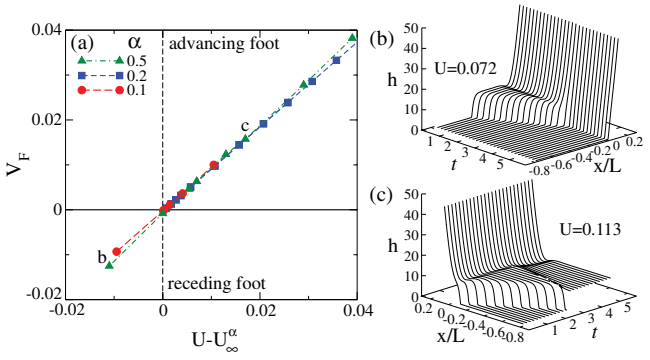

FIG. 3 (color online). (a) Advancing and receding footlike structures are characterized by the dependence of the velocity V_F of the front that connects the ultrathin coating layer with the foot plateau of height h_f on the velocity difference $U - U_\infty^\alpha$ where U_∞^α changes with the plate inclination α. Note that the curves for various α collapse onto a master curve, $V_F \approx U - U_\infty^\alpha$. Panels (b) and (c) show for $\alpha = 0.5$ the time evolution [35] of a receding and an advancing foot, respectively, at values of U indicated by small letters in panel (a). The evolution in (b) converges to a steady simple meniscus, while in (c) the foot advances with constant speed until its tip reaches the domain boundary.

(c) At a second critical $\alpha = \alpha_2 \approx 2.42$, the bifurcation diagram dramatically changes. Above α_2 the family of steady menisci that is connected to $U = 0$ does not anymore diverge at a limiting velocity U_∞. Instead of a protruding foot of increasing length that unbinds from the meniscus one finds a hysteretic transition [in Fig. 2(c) between $U = 0.2$ and 0.3] towards a coating layer whose thickness homogeneously increases with increasing U; i.e., the layer surface unbinds from the substrate in a *discontinuous dynamic wetting transition*.

(d) With increasing α the hysteresis of the discontinuous transition becomes smaller until at a third critical $\alpha = \alpha_3 \approx 5.92$ the two saddle-node bifurcations annihilate in a hysteresis bifurcation as further illustrated in Fig. 4. For all $\alpha > \alpha_3$ one finds a *continuous dynamic wetting transition*. As in cases (c) and (d), at large U the coating layer thickness follows the power law $h_\infty \propto U^{2/3}$, we identify these unbinding states as Landau-Levich films [9]. The critical velocity, where the transition between the microscopic and macroscopic layer occurs, scales as $\alpha^{3/2}$.

Note that the dynamic emptying transitions of cases (a) and (b) and the crossover between them are also observed employing a slip model [19,21] and for case (b) the foot structure and even an unstable part of the snaking curve have been experimentally observed [8,16]. The slip model, however, does not take the mesoscale wetting behavior into account and is therefore unable to describe the discontinuous and continuous dynamic wetting transitions of cases (c) and (d), respectively, as these represent transitions between the topologically different meniscus and film solutions. Note, that slip models that incorporate mesoscale wetting behavior exist [37,38] and could in the future be used to analyze drawn menisci with both effects present.

To summarize our findings, we present in Fig. 5 a phase diagram in the (U, α) plane as obtained by tracking the main occurring saddle-node bifurcations (black solid lines)

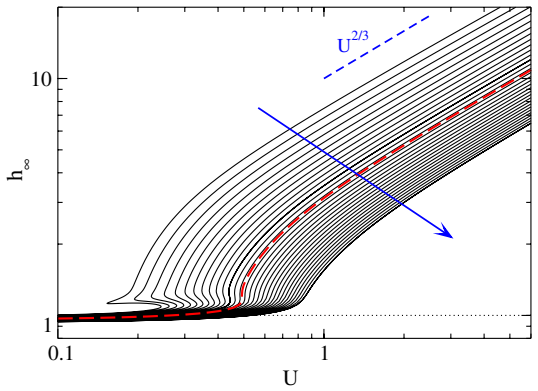

FIG. 4 (color online). The film height of thick (macroscopic) coatings scales following the Landau-Levich law, $h_\infty \propto U^{2/3}$ for $U \gtrsim 1$. The shown curves correspond to equidistant inclination angles with $\alpha \in [2.42, 10]$ and $\Delta\alpha = 0.25$. The arrow indicates increasing α. The thick dashed line indicates the transition from discontinuous to continuous dynamic wetting transitions at α_3.

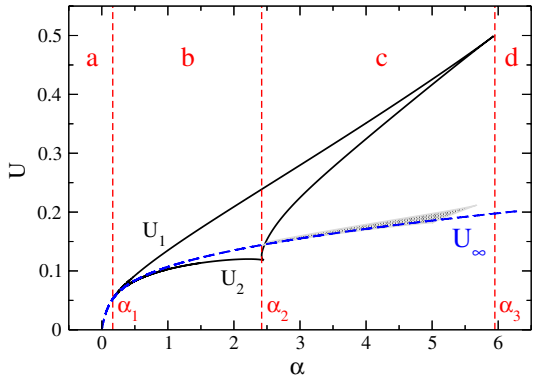

FIG. 5 (color online). The phase diagram in the (U, α) parameter plane shows regions of different behavior that are limited by the loci of (i) saddle-node bifurcations of steady film surface profiles (black solid lines) and (ii) by the dependence of the limiting velocity U_∞ on α (blue dotted line). The existence of an additional solution family close to U_∞ in region (c) is indicated by grey shading.

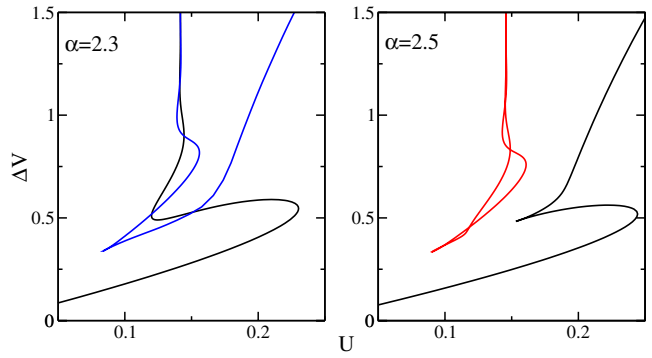

FIG. 6 (color online). Detail of the transition from case (b) to (c) and full bifurcation diagram gathering the two families of solutions. One observes that the transition occurs via a reverse–necking bifurcation at $\alpha = \alpha_2$ and that Landau-Levich films are present below α_2.

and the limiting velocity U_∞ (blue dashed line). In region (a), i.e., for $0 < \alpha < \alpha_1$, ultimately a simple or extended (footlike) steady meniscus is found for $U < U_\infty$ while for $U > U_\infty$ the foot advances at constant speed $V_F \approx (U - U_\infty)$ [cf. Fig. 3(a)]. In region (b), i.e., for $\alpha_1 < \alpha < \alpha_2$, multiple stable foot solutions exist for U between the two solid lines. However, for each U with $U_2 > U > U_\infty$ there is always a maximal stable foot length $L^-_{\max}$ towards which a longer foot will retract. For each U with $U_\infty > U > U_1$ there is always a maximal unstable steady foot length $L^+_{\max}$ beyond which the foot will advance continuously. $L^-_{\max}$ [$L^+_{\max}$] logarithmically diverges as U approaches U_∞ from below [above].

In region (c), i.e., for $\alpha_2 < \alpha < \alpha_3$, the lines of saddle-node bifurcations limit a region where initial conditions decide whether an ultrathin layer or a macroscopic Landau-Levich coating is obtained. Below [above] the hysteresis range one only finds the ultrathin [Landau-Levich] coating. In region (d), i.e., for $\alpha > \alpha_3$, the change between the two coating types is continuous.

Finally, we highlight some further important facts. The crossover between regions (a) and (b) is related to a change of the character of the spatial eigenvalues (EVs) of a flat film of foot height [21,32]: In region (a) all EVs are real while in region (b) one is real and the other two are complex conjugate. The crossover between regions (c) and (d) results from a hysteresis bifurcation where two saddle-node bifurcations annihilate. However, the crossover between regions (b) and (c) that results in the strong qualitative change, from a dynamic emptying to a dynamic wetting transition, cannot be understood by considering a single branch of profiles. Instead, the crossover results from a reconnection that involves two solution branches (see Fig. 6). In consequence, in the fine grey band around U_∞ in region (c) [Fig. 5], there exist various stable extended meniscus profiles. They correspond to the left branch in Fig. 6(b). Experimentally, they might only be obtained through a careful control of the setup at specific initial conditions. Figure 6 also explains why Landau-Levich film states may be dynamically accessed even at $\alpha < \alpha_2$ (cf. Fig. 3).

To conclude, we have shown that a long-wave mesoscopic hydrodynamic description of the coating problem for a plate that is drawn from a bath allows one to identify several qualitative transitions if wettability is modeled via a Derjaguin pressure. As a result we have distinguished four dynamic unbinding transitions, namely continuous and discontinuous dynamic emptying transitions and discontinuous and continuous dynamic wetting transitions. These dynamic transitions are out-of-equilibrium equivalents of well-known equilibrium emptying and wetting transitions. Besides features known from equilibrium, our analysis has uncovered important features that have no equivalents at equilibrium. A future study of the influence of fluctuations might allow one to understand which surface profile is selected in the multistable regions.

We acknowledge support by the EU via the FP7 Marie Curie scheme (ITN MULTIFLOW, PITN-GA-2008-214919).

*mgalvagno@gmail.com
†u.thiele@uni-muenster.de; http://www.uwethiele.de

[1] D. Bonn, J. Eggers, J. Indekeu, J. Meunier, and E. Rolley, Rev. Mod. Phys. **81**, 739 (2009).
[2] A. O. Parry, C. Rascon, E. A. G. Jamie, and D. G. A. L. Aarts, Phys. Rev. Lett. **108**, 246101 (2012).
[3] T. Podgorski, J.-M. Flesselles, and L. Limat, Phys. Rev. Lett. **87**, 036102 (2001).
[4] U. Thiele, K. Neuffer, M. Bestehorn, Y. Pomeau, and M. G. Velarde, Colloids Surf. A **206**, 87 (2002).
[5] M. B. Amar, L. J. Cummings, and Y. Pomeau, Phys. Fluids **15**, 2949 (2003).

[6] J. H. Snoeijer and B Andreotti, Annu. Rev. Fluid Mech. **45**, 269 (2013).
[7] T. D. Blake and K. J. Ruschak, Nature (London) **282**, 489 (1979).
[8] G. Delon, M. Fermigier, J. H. Snoeijer, and B. Andreotti, J. Fluid Mech. **604**, 55 (2008).
[9] L. Landau and B. Levich, Acta Physicochim. URSS **17**, 42 (1942); Reprinted in *Dynamics of Curved Fronts*, edited by P. Pelce (Academic Press, London, 1988), edition number 1.
[10] B. Derjaguin, Acta Physicochim. USSR **39**, 1316 (1943).
[11] S. D. R. Wilson, J. Eng. Math. **16**, 209 (1982).
[12] A. Münch and P. L. Evans, Physica (Amsterdam) **209D**, 164 (2005).
[13] F. S. Goucher and H. Ward, Philos. Mag. **44**, 1002 (1922).
[14] P. Groenveld, Chem. Eng. Sci. **25**, 33 (1970).
[15] J. H. Snoeijer, G Delon, M Fermigier, and B Andreotti, Phys. Rev. Lett. **96**, 174504 (2006).
[16] J. H. Snoeijer, J. Ziegler, B. Andreotti, M. Fermigier, and J. Eggers, Phys. Rev. Lett. **100**, 244502 (2008).
[17] M. Maleki, M. Reyssat, F. Restagno, D. Quere, and C. Clanet, J. Colloid Interface Sci. **354**, 359 (2011).
[18] J. Eggers, Phys. Rev. Lett. **93**, 094502 (2004).
[19] J. H. Snoeijer, B. Andreotti, G. Delon, and M. Fermigier, J. Fluid Mech. **579**, 63 (2007).
[20] T. S. Chan, J. H. Snoeijer, and J. Eggers, Phys. Fluids **24**, 072104 (2012).
[21] J. Ziegler, J. H. Snoeijer, and J. Eggers, Eur. Phys. J. Spec. Top. **166**, 177 (2009).
[22] P.-G. de Gennes, Rev. Mod. Phys. **57**, 827 (1985).
[23] Special issue "Discussion and Debate: Wetting and Spreading Science - quo vadis?", edited by M. G. Velarde [Eur. Phys. J. Special Topics **197** (2011)].
[24] N. Savva and S. Kalliadasis, Europhys. Lett. **94**, 64004 (2011).
[25] U. Thiele, in *Thin Films of Soft Matter*, edited by S. Kalliadasis and U. Thiele (Springer, Wien, 2007), pp. 25–93.
[26] U. Thiele, J. Phys. Condens. Matter **22**, 084019 (2010).
[27] A. Oron, S. H. Davis, and S. G. Bankoff, Rev. Mod. Phys. **69**, 931 (1997).
[28] For the dimensional disjoining pressure $\Pi = -A/h^3 + B/h^6$, with Hamaker constant $A > 0$ and short-range interaction strength $B > 0$, the equilibrium precursor height and contact angle are $h_{\mathrm{eq}} = (B/A)^{1/3}$ (i.e., the scaled precursor height is $h_p = 1$) and $\theta_{\mathrm{eq}} = \sqrt{3A/5\gamma h_{\mathrm{eq}}^2}$ (i.e., the scaled equilibrium contact angle is $\sqrt{3/5}$), respectively. The velocity scale, gravity number, and the scaled inclination angle are given by $3\tau/\ell$, $G = \rho g h_{\mathrm{eq}}^4/A$, and $\alpha = (\ell/h_{\mathrm{eq}})\tilde{\alpha} = O(1)$, respectively, where ρ, η, and γ are the density, viscosity, and surface tension of the liquid, and g is gravitational acceleration. The physical plate inclination angle $\tilde{\alpha}$ is assumed to be small, thereby ensuring uniform validity of the long-wave model in the precursor, meniscus, and bath region. We use $G = 0.001$.
[29] V. M. Starov and M. G. Velarde, J. Phys. Condens. Matter **21**, 464121 (2009).
[30] L. M. Pismen, Colloids Surf. A **206**, 11 (2002).
[31] Here, $\xi dx \approx (1/2)[1 + (\partial_x h)^2] ds$ is the surface area element in long-wave approximation and $f(h)$ is an appropriately defined energy containing terms related to wettability and gravity. Note that in the wetting literature $F[h]$ is called "Hamiltonian" as it may be derived from a microscopic Hamiltonian. However, thermodynamically it is a free energy, while mathematically it represents a Lyapunov functional.
[32] D. Tseluiko, M. Galvagno, and U. Thiele, Eur. Phys. J. E (in press).
[33] H. A. Dijkstra, F. W. Wubs, A. K. Cliffe, E. Doedel, I. F. Dragomirescu, B. Eckhart, A. Y. Gelfgat, A. Hazel, V. Lucarini, A. G. Salinger, E. T. Phipps, J. Sanchez-Umbria, H. Schuttelaars, L. S. Tuckerman, and U. Thiele, Commun. Comput. Phys. **15**, 1 (2014).
[34] We define the measure for the foot length $L_f \propto \Delta V/(h_f - h_\infty)$, where h_f is the foot height and h_∞ the coating film height.
[35] The time simulations employ a second order central finite difference scheme in space and a variable-order and variable-step backward differentiation algorithm in time.
[36] Y. P. Ma, J. Burke, and E. Knobloch, Physica D (Amsterdam) **239D**, 1867 (2010).
[37] K. Kargupta, A. Sharma, and R. Khanna, Langmuir **20**, 244 (2004).
[38] A. Münch, B. Wagner, and T. P. Witelski, J. Eng. Math. **53**, 359 (2005).